3B2v8.06a/w (Dec 5 2003).51c + model
PHYSA : 9736
Prod.Type:FTP
pp.1–13(col.fig.:NIL)
ED:S.AmjadP
PAGN:TNN SCAN:

ARTICLE IN PRESS

Available online at www.sciencedirect.com
SCIENCE DIRECT®

ELSEVIER

Physica A ▮ (▮▮▮▮) ▮▮▮–▮▮▮

PHYSICA A

www.elsevier.com/locate/physa

Synchronization in systems with bimodal dynamics

A.P. Kuznetsov[a], E. Mosekilde[b], L.V. Turukina[a,*]

[a]*Institute of Radio Engineering and Electronics, Russian Academy of Sciences, Saratov Branch, Zelenaya 38, Saratov, 410019, Russian Federation*

[b]*Department of Physics, The Technical University of Denmark, 2800 Kgs.Lyngby, Denmark*

Received 1 December 2005; received in revised form 13 March 2006

Abstract

Considering a prototypic model of a bimodal oscillator we first investigate the synchronization of the internal time scales for a system with interacting fast and slow oscillatory modes. Particular emphasis is given to the transition between mode-locked and mode-unlocked chaos. It is shown that this transition involves a homoclinic bifurcation in which the synchronized chaotic attractor loses its band structure. For two coupled bimodal oscillators we illustrate the presence of separate synchronization regions for the fast and the slow modes. The dependence of these regions on the mismatch and coupling parameters is studied.

1. Introduction

The collective motion of systems with two or more interacting nonlinear oscillators is of significant interest in many areas of science and technology [1–3]. Particularly interesting is the case where the uncoupled oscillators display complex dynamics [4–6]. This situation has been investigated experimentally, for instance, for two coupled chaotically oscillating lasers [7], for a system of globally coupled electrochemical reactors [8], and for neighboring nephrons in hypertensive rats [9]. Synchronization in systems of nearly identical chaotic oscillators has been extensively studied in connection with their possible use for secure communication [10,11]. Here, some of the main questions of concern relate to the ability of the oscillators to synchronize if they are started out of synchrony and to the stability of the synchronized state in the presence of noise or of small parameter mismatches [12,13].

It appears that the classical concept of synchronization, related to the locking of the basic frequencies and instantaneous phases for coupled oscillators also applies to a certain class of chaotic systems with nonidentical parameters, particularly to oscillators for which the basic frequencies are clearly distinguishable in the power spectrum [2,14,15]. This is typically the case for systems such as the Roessler oscillator where the transition to chaos occurs via a cascade of period-doubling bifurcations.

While the dynamics of systems with one oscillatory mode is relatively well understood, the synchronization in systems with two and more oscillatory modes (time scales) is less studied. Systems of this type are

*Corresponding author.
E-mail address: ludmila@forpost.ru (L.V. Turukina).

0378-4371/$ - see front matter © 2006 Published by Elsevier B.V.
doi:10.1016/j.physa.2006.03.028

encountered in various engineering applications, for instance when systems with fast dynamics are subjected to a slow modulation, or in systems where brief bursts of oscillatory activity are interrupted by longer periods of more quiet dynamics.

Living systems also exhibit a great variety of different rhythms of significance to the regulation of their normal physiological processes. Hormonal secretion provides a great number of examples with the release of insulin, for instance, displaying pronounced ultradian (2–3 h) cycles [16,17]. The release of insulin also displays a faster, 9–15 min rhythm, which is believed to be important to the regulation of metabolic processes in the liver [18]. At the same time, the circadian (24 h) rhythm modulates the ultradian variations providing, for instance, for a particularly strong ultradian pulse of insulin in the early morning [17].

Rhythmic processes also play a significant role at the cellular level, both for the regulation of the functions of the individual cells and for the inter-cellular communication. The insulin producing beta-cells in the pancreas, for instance, are known to show variations in their hormonal release that are directly correlated with complicated patterns of bursts and spikes in their membrane potentials [18]. Interaction between the beta-cells takes place via a variety of different mechanisms, including, the short-range diffusive exchange of ions and small molecules through gap junctions [19] and the response of the individual cell to variations in the inter-cellular calcium concentration produced by the bursting activity of adjacent cells [20]. Hence, one can observe synchronization of the bursting activity between neighboring cells [21] as well as waves of cytoplasmic calcium propagating across larger groups of pancreatic cells [22].

In a series of papers [9,23,24], Holstein-Rathlou et al. have developed a detailed model of the mechanisms by which the individual functional unit (the nephron) in the kidney regulates the incoming blood flow. This regulation involves a so-called tubuloglomerular feedback (TGF) mechanism by which the diameter of the blood vessel is regulated in response to the salt concentration in the fluid leaving the nephron. The TGF mechanism represents a negative feedback. However, by virtue of delays (associated primarily with the flow of fluid through the loop of Henle) and of a relatively high loop gain, the regulation tends to be unstable and to excite self-sustained oscillations in the nephron pressures, flows and concentrations with a period of about 30 s. The response of the afferent arteriole to the TGF signal is strongly nonlinear and oscillates with a period of about 6 s and a relatively small damping. This allows for a significant number of nonlinear dynamic phenomena to occur, and experiment on rats have shown (i) that neighboring nephrons tend to synchronize their pressure oscillations, (ii) that the synchronization can be either in-phase or out-of-phase, and (iii) that the synchronization may be maintained when, at high blood pressures, the tubular oscillations become chaotic.

A more detailed description of these complex, multimode synchronization phenomena represents an obvious challenge to the theory of nonlinear dynamical systems. In a couple of recent publications, Postnov et al. have discussed the role of multistability in the transition to chaotic phase synchronization [25] and the complex phase dynamics of coupled bursters [26]. Postnov et al. [27] have also discussed multimode synchronization in a simplified model of two coupled nephrons. The purpose of the present paper is to analyze a prototypic model of a system of interacting two-mode oscillators in order to study the intra- and inter-mode synchronization phenomena in a more generic framework.

The model we shall consider consists of two coupled nonlinear oscillators: a Van der Pol oscillator and a Duffing oscillator with a displaced equilibrium point. We first study synchronization between the two time scales (fast and slow modes) in the individual system and investigate the transition between mode-locked and mode-unlocked chaotic regimes which takes place in such a system. We show that this transition is associated with a homoclinic bifurcation (a crisis) in which the mode-locked chaotic attractor loses its multiband structure as it collides with an unstable periodic orbit. As long as the chaotic attractor maintains its multiband structure, the dynamics of the system is characterized by a significant degree of regularity, and the internal winding number remains rational and constant through a variety of bifurcations. When the multiband structure is lost, the two oscillatory modes also lose their internal synchronization. It is interesting to note, however, that loss of synchronization has a precursor in the form of fluctuations in the numerically calculated rotation number as the distance between the chaotic bands becomes sufficiently small. For coupled systems that individually demonstrate mode-locked chaos, we study the synchronization regions for the fast and slow oscillatory modes separately and investigate their dependence on the mismatch and coupling parameters of the systems.

2. Dynamics of the single system

Let us consider a simple system with two-mode dynamics described by the two coupled oscillators:

$$\ddot{x} + k\dot{x} + x^3 = B(y + a), \tag{1}$$

$$\ddot{y} - (\alpha - y^2)\dot{y} + y = Cx. \tag{2}$$

The first equation is a form of Duffing oscillator [28] with the feedback By from the second equation playing the role of a forcing term. k is the damping coefficient. The second equation is a Van der Pol oscillator modulated by the feedback Cx from the Duffing oscillator. The Van der Pol oscillator generates self-sustained oscillations with an amplitude determined by the dissipation parameter $\alpha > 0$. For small values of C, our bimodal oscillator may be considered as a Duffing oscillator driven by the periodic force term produced by the Van der Pol oscillator. At sufficiently large values of C, however, the feedback from the Duffing oscillator quenches the oscillations in the Van der Pol oscillator, and the system (1)–(2) enters a state of oscillator death where a stable equilibrium point is the only stationary state.

Under variation of the parameters k and B, the Duffing oscillator is known [28] to produce a complicated structure of local and global bifurcations with different transitions to chaos and with regions of coexisting attractors and fractal basin boundaries.

In the coarsest interpretation [29], this structure may be considered to arise from a series of resonances in which the Duffing oscillator completes $m = 1, 2, 3$ internal oscillations for each period of the external forcing. In these resonances, the odd modes ($m = 1, 3, 5$) are symmetric whereas the even modes ($m = 2, 4, 6$) are asymmetric. Symmetry breaking pitchfork bifurcations delineate regions in parameter space where strong even modes occur, and regions where high amplitude odd overtones occur are delineated by saddle-node bifurcations. With increasing forcing amplitude, the asymmetric solutions generated in the pitchfork bifurcations typically proceed through period-doubling bifurcations to chaos.

By introducing the constant term Ba on the right-hand side of Eq. (1), we have shifted the equilibrium point of the Duffing oscillator away from $x = 0$. In this way we have broken the symmetry of the original equation, and the system (1)–(2) no longer produces symmetric modes. However, we can still have $m = 1, 2, 3, \ldots$ resonances with even as well as with odd internal oscillations of the Duffing oscillator per oscillation of the Van der Pol oscillator. The idea of introducing the constant forcing term is to obtain a situation in which the Duffing oscillator only produces rapid oscillations for positive values of x. The model will then reproduce the behavior observed for the nephron model [3] in a qualitative manner. Fig. 1 shows typical time series for the dynamical variables x and y in a chaotic regime with fast and slow oscillatory modes. Here, $B = 1.66$ and $C = 0.4392$. For the remaining parameters we have chosen the values $k = 0.4$, $\alpha > 0$ and $a = 0.8$. These values will be kept constant throughout the study.

Fig. 2 provides an overview of the main dynamical regimes for the bimodal oscillator in the (B, C) parameter plane. To illustrate some of the typical attractors observed in the system, the figure also shows a number of $(x, \dot{x})$ phase projections for selected combinations of the two coupling parameters. In the chart of the dynamical modes we have used a gray tone palette to distinguish between various regions with periodic and chaotic solutions: period-1 oscillations (i.e., oscillations that repeat themselves after a single cycle of the driving Van der Pol oscillator) are indicated in white, period-2 oscillations in light gray, period-4 oscillations in dark gray, and chaos and longer-period oscillations in black. Notice, that the region of oscillator death is also marked dark gray.

As presented in Fig. 2, the different dynamical regions appear as islands, each representing a structure of partially overlapping period-doubling cascades developed from a specific resonance in the bimodal oscillator. Fig. 2(c) for instance, depicts a 1:3 solution with three fast oscillations per slow oscillation. Fig. 2(b) shows the corresponding 2:6 solution, and Fig. 2(a) shows a chaotic attractor developed from the 2:6 solution via a period-doubling cascade. It seems reasonably to assume that this attractor on the average also maintains a ratio of slow to fast oscillations close to 1:3.

To examine this conjecture we need to calculate the rotation number for the bimodal oscillator. The simple substitution $\dot{x} = u$ and $\dot{y} = v$ can be used to convert Eqs. (1)–(2) into a set of four coupled first order differential equations. To calculate the frequency ratio of the two modes we determine the mean return times

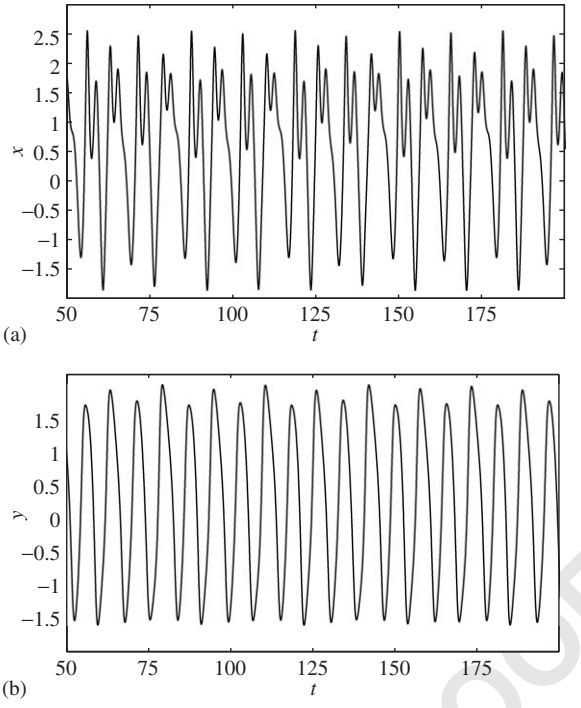

Fig. 1. Typical time-series for the dynamical variables x and y in a chaotic regimes with fast and slow oscillations. $k = 0.4$, $\alpha = 1.0$, $a = 0.8$, $B = 1.66$ and $C = 0.4392$.

$\langle \tau_u \rangle$ and $\langle \tau_y \rangle$ of the trajectory in four-dimensional phase space to two Poincaré sections defined, respectively, by $u = 0$ and $y = 0$ in the (x, u) and (y, v) subspaces. We can then define the rotation number as

$$r = \frac{\langle \tau_u \rangle}{\langle \tau_y \rangle}, \tag{3}$$

where the time average $\langle\rangle$ has to be taken over a large number of oscillations. During all (this and following) numerical computations we used trajectories more then 5000 periods long.

Fig. 3 shows a calculation of the rotation number as a function of C in a vertical scan of the (B, C) parameter plane of Fig. 2 for $B = 1.66$. (A plot of the rotation number as a function of B for fixed C has a very similar form.) Fig. 3 also shows the brute force bifurcation diagram corresponding to the depicted variation of r. This helps us to identify specific dynamical regions with their rotation numbers.

One can distinguish four different intervals of constant rotation numbers in the scan of Fig. 3 in the right most interval $(0.585 < C < 0.65)$, $r = 0.3333\ldots$. This corresponds to 1:3 synchronization between the two modes. In this interval, the bifurcation diagram only shows a single period-doubling bifurcation (to a 2:6 oscillation) followed by a reverse period-doubling bifurcation. These bifurcations obviously do not influence the relative frequencies of the two modes. The two intermediate intervals have $r \cong 0.4$ and $r \cong 0.4448$, respectively, corresponding to 2:5 and 4:9 synchronous solutions. Fig. 4 shows time plots for the x variable of the corresponding stationary states. Each of the two intervals with 2:5 and 4:9 synchronization again shows a single period-doubling bobble, indicating that the scan only passes through peripheral regions of the various islands. The abrupt jump in the observed behavior for $C \cong 0.5155$, and the associated jump in the rotation number, are classical signatures of overlapping islands. Thus, in an interval to the left of this point the system displays two coexisting solutions. This is easily verified by performing a scan in the opposite direction (i.e., for decreasing values of C).

Considerable more interesting are the variations that occur in the interval $0.4 < C < 0.5$ and in the chaotic region around $C = 0.59$. Fig. 5 shows an enlargement of the first of these regions. This figure also displays 3D phase projections of some of the characteristic attractors we meet in the scan. With increasing C, the first

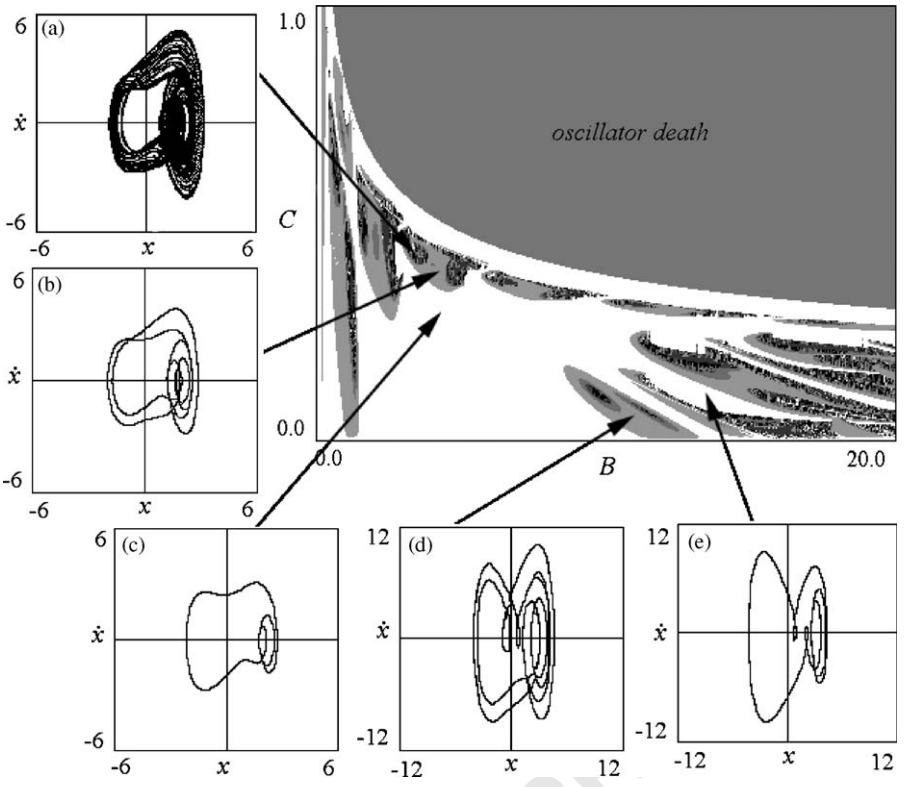

Fig. 2. Chart of the dynamical regimes of the system (1)–(2) in the (B, C) parameter plane for the next values of the parameters: $k = 0.4$, $\alpha = 1.0$ and $a = 0.8$. The $(x, \dot{x})$ phase projection of the attractors of system (1)–(2) is present in this figure too. They are plotted at the next values of the parameters: (a) $C = 0.4253$ and $B = 3.431$; (b) $C = 0.4099$ and $B = 3.243$; (c) $C = 0.3287$ and $B = 4.042$; (d) $C = 0.0771$ and $B = 15.28$; (e) $C = 0.0499$ and $B = 10.796$.

attractor to be observed is the 2:4 mode-locked solution that exists around $C = 0.41$. In this state, the bimodal oscillator exhibits four fast oscillations for every two slow oscillations. At $C \cong 0.42$, the 2:4 solution bifurcates into a 4:8 mode-locked solution (Fig. 5(b)), and the cascade of period-doubling bifurcations continues to finally accumulate near $C = 0.44$. The rotation number r remains constant and equal to 0.5 through the entire cascade. Moreover, the rotation number continues to be precisely 0.5 as the scan is extended into the chaotic regime with its infinite sequences of homoclinic bifurcations and dense set of periodic windows. Fig. 5(c) shows an example of the mode-locked chaotic attractor that exists in this region. Because of the multiband structure of the attractor, the dynamics of the system maintains a considerable degree of regularity, and there are always two fast oscillations for each slow oscillation.

As C exceeds 0.455 one can start to observe a certain fluctuation in the rotation number. This fluctuation is a variation of rotation number as a function of parameter C and do not depend on number of computations. The transition from a constant and well-defined rotation number to a slightly fluctuating rotation number is likely to be the result of occasional jumps from band to band in the chaotic attractor as these bands, with increasing C, approach one another. In a real physical or biological system, the occurrence of this transition will depend on the noise level. It is important to note, however, that the band structure of the chaotic attractors allows us to observe mode-locked chaos at finite noise amplitudes.

At $C \cong 0.4595$, the rotation number finally starts to decrease rapidly, indicating that the average number of fast oscillations per slow oscillation starts to increase. This happens simultaneously while the band-merging bifurcation in which the two-band chaotic attractor is transformed into a one-band attractor. After the merger of the two bands, the system can no longer provide the separation required to maintain a fixed rotation number. Before the band-merging transition, we have 1:2 mode-locked chaotic dynamics, and after the transition we have unlocked chaos. We supposed that merging of the two bands takes place via a homoclinic

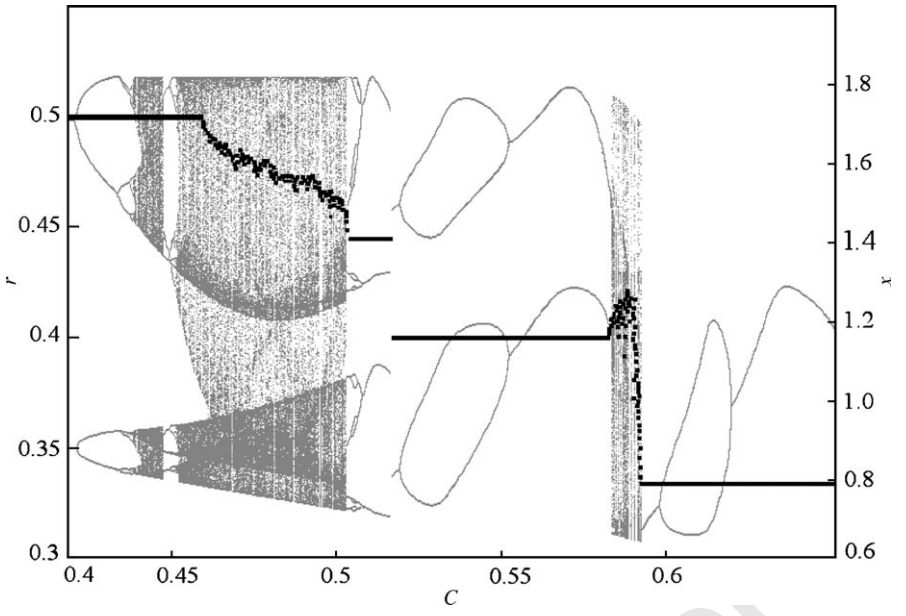

Fig. 3. Numerically calculated rotation number r as function of parameter C for system (1)–(2) at $k = 0.4$, $\alpha = 1.0$, $a = 0.8$ and $B = 1.66$. It is shown by the black curve. The bifurcation diagram is also shown in this figure. Intervals of constant rotation number corresponds to synchronization between the fast and slow modes.

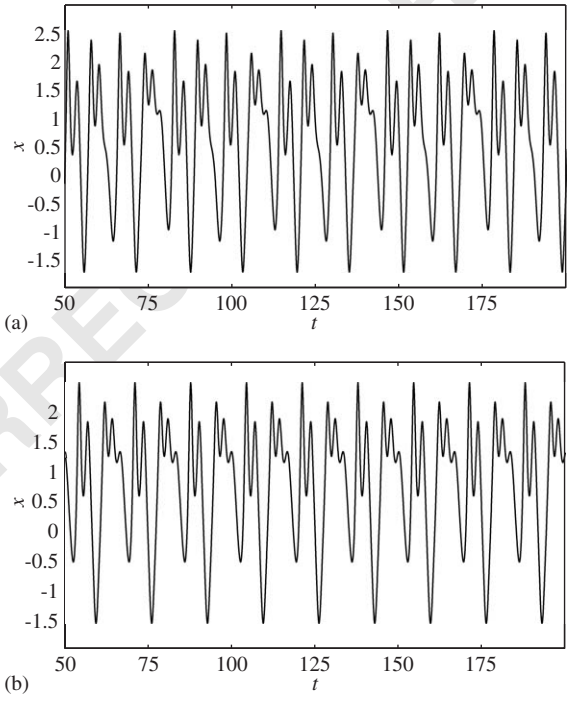

Fig. 4. Time-series for the dynamical variable x of system (1)–(2) corresponded to rotation numbers $r = 0.4448\ldots$ (a) and $r = 0.4$ (b).

bifurcation in which the bands collide with the insert (stable manifold) to the unstable 1 cycle. This scenario is typical for systems demonstrating band-merging transition after a cascade of period-doubling bifurcations [30].

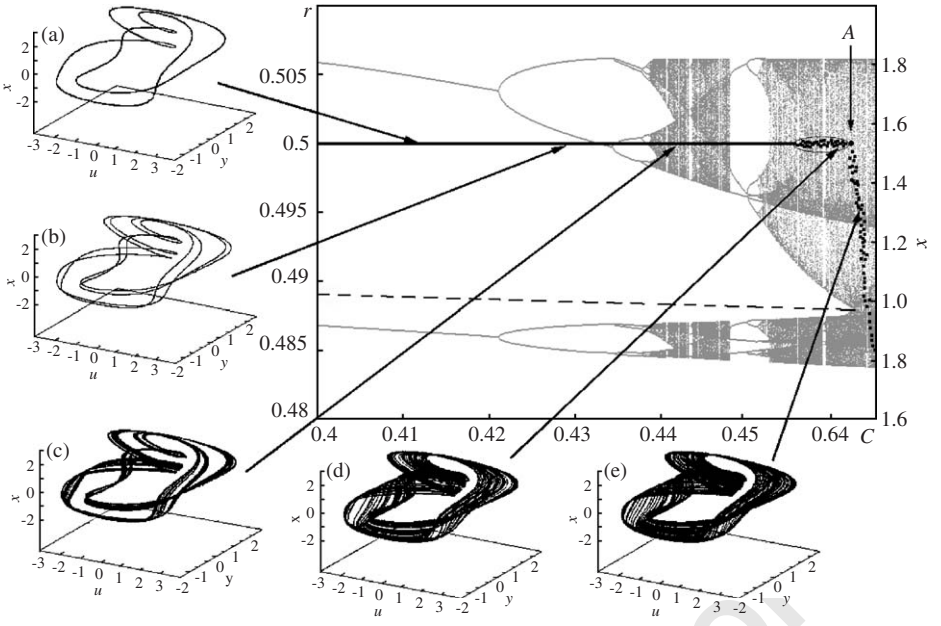

Fig. 5. Zoom of part of the diagram presented in Fig. 3. The unstable period 1 cycle is shown by the dotted line. The corresponding 3D phase projections are present on this figure too. They are plotted at the next values of the parameters: $k = 0.4$, $\alpha = 1.0$, $a = 0.8$, $B = 1.66$ and $C = 0.4$ (a), $C = 0.43$ (b), $C = 0.4392$ (c), $C = 0.457$ (d), $C = 0.462$ (e).

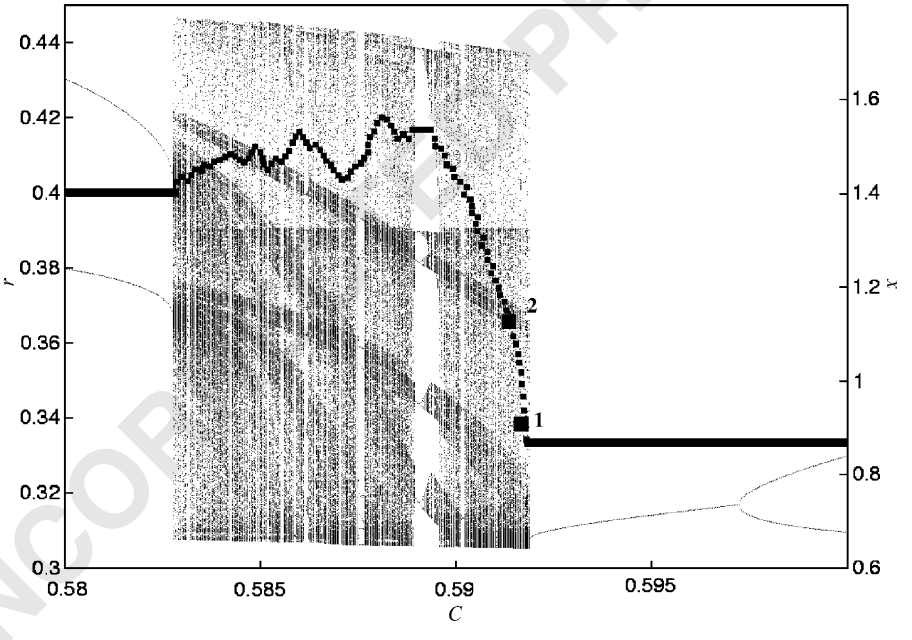

Fig. 6. Zoom of part of the diagram presented in Fig. 3. The right part of Fig. 3 where rotation number r takes values of $r = 0.4$ and decrease to $r = 0.333333\ldots$ is shown. The points denoted 1 (with $C = 0.591885$) and 2 (with $C = 0.5915$) corresponded to mode-locked and mode-unlocked chaotic attractors.

Fig. 6 shows a blowup of the chaotic region near $C = 0.59$ (see Fig. 3). The sequence of small black squares represents the numerically calculated rotation numbers as a function of C. As before, the brute force bifurcation diagram is also shown in the figure to allow us to identify the rotation numbers with the various modes. To the left in Fig. 6, the rotation number starts at $r = 0.40$, corresponding to the rotation number of

the 2:5 mode-locked periodic solution, and in the other end of the chaotic regime r is only approximately 0.3333..., corresponding to the rotation number of the mode-locked 2:6 solution. In the intermediate interval, while fluctuating significantly, the rotation number rises first to about 0.42 and then decrease to 0.333. The initial rise of r represents a reduction in the average number of fast oscillations per slow oscillation. In spite of the observed fluctuations we conclude that the rotation number in the chaotic regime approaches the rotation numbers for the adjacent periodic orbits in both ends. The rotation number also has to pass through the appropriate rational values in the periodic windows. In particular, we notice that the rotation number passes through 0.4167 in the 5:12 periodic window immediately below $C = 0.59$.

Let us consider the two points denoted 1 and 2 in Fig. 6 in a little more detail. The first point (with $C = 0.591885$) falls near the boundary to the 2:6 periodic window, and the numerically calculated rotation number for the corresponding chaotic attractor is 0.3333. The second point (with $C = 0.5915$) falls in the middle of the chaotic regime, and the (presumably irrational) rotation number is here $r \cong 0.36$.

Fig. 7 shows 2D and 3D phase projections of the two chaotic attractors. In point 1 (Figs. 7(a) and (c)), the attractor displays a clear 3-band structure, and the regularity of this band structure is sufficiently strong to ensure that there is always three fast oscillations per slow oscillation. This band structure is also notable in the bifurcation diagram of Fig. 6. However, as we move a little to the left, the chaotic attractor undergoes a crisis, and the trajectory spreads over a large r range. This crisis is likely to occur in analogy with the well-known crisis of the chaotic 3-band attractor in the logistic map [30]. In the thrice interacted logistic map, the crisis takes place in a homoclinic bifurcation when the second iterate of the critical point maps into the unstable period-3 cycle. In our case, by analogy, the crisis occurs when the chaotic 3-band attractor collides with the insert of the unstable 1:3 cycle. (Band merging across the unstable 2:6 cycle has already occurred.)

Again we can conclude that the transition from mode-locked chaos to unlocked chaos involves a homoclinic bifurcation that destroys the regular band structure of the attractor.

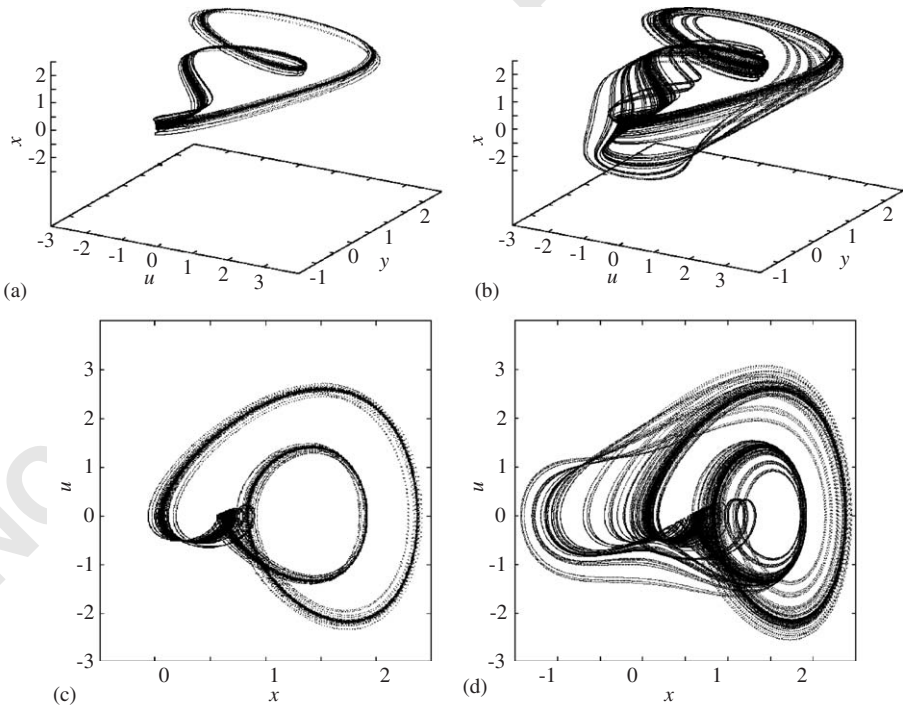

Fig. 7. 2D and 3D phase projections of the attractor for system (1)–(2). The projections are plotted for the points 1 ($C = 0.591885$) (a, c) and 2 ($C = 0.5915$) (b, d) from Fig. 6. The first point corresponded to mode-locked chaotic attractor with rotation number $r = 0.3333\ldots$. The second point corresponded to mode-unlocked chaotic attractor and rotation number is $r \cong 0.36$. All other parameters are fixed at $k = 0.4$, $\alpha = 1.0$, $a = 0.8$, $B = 1.66$.

In the point 2 of Fig. 6, the chaotic attractor no longer possesses a clear band structure (see Figs. 7(b) and (d)), but some of the slow oscillations encompass two fast oscillations while others give time for three fast oscillations. Hence, chaotic mode locking no longer occurs, and the rotation number is in general irrational.

3. Synchronization of two bimodal oscillators

Now we consider synchronization of two coupled systems (1)–(2), individually demonstrating mode-locked chaos. Using a model derived more directly from the original biological system (nephron pressure and flow control), Postnov et al. [27] have considered a somewhat similar problem. In their work two systems with two-mode dynamics, individually demonstrating mode-locked chaos, were coupled via a slow variable and the presence of synchronization between subsystems was shown for this type of coupling. In the present work we shall consider coupling via a fast variable x. We introduce a simple one-variable-difference coupling term into Eq. (1) with strength μ into Eq. (2). This is perhaps the simplest way to couple two subsystems. However, this type of coupling leads to a situation, in which any variation of the frequency of the individual system (1)–(2) will change not only the main frequency of oscillations but also the type of chaotic regime observed in each subsystem separately. The idea is to couple systems (1)–(2) in such a way, that they will individually demonstrate the same type of chaotic regime in some range on parameters (frequency mismatch and coupling strength). As suggested, for instance, by Anishenko et al. [6], this can be achieved by introducing the additional scale factor ε in the left-hand side of the second subsystem: $\varepsilon = 1.0$ corresponds to the case of identical systems, and $\varepsilon \neq 1.0$ introduces a mismatch between the two subsystems. Then we arrive at the following system of the equations:

$$\begin{aligned} \dot{x}_1 &= u_1 + \mu(x_2 - x_1), \\ \dot{u}_1 &= -ku_1 - x_1^3 + B(y_1 + a), \\ \dot{y}_1 &= v_1, \\ \dot{v}_1 &= (\alpha - y_1^2)v_1 - y_1 + Cx_1, \end{aligned} \tag{4}$$

$$\begin{aligned} \varepsilon\dot{x}_2 &= u_2 + \mu(x_1 - x_2), \\ \varepsilon\dot{u}_2 &= -ku_2 - x_2^3 + B(y_2 + a), \\ \varepsilon\dot{y}_2 &= v_2, \\ \varepsilon\dot{v}_2 &= (\alpha - y_2^2)v_2 - y_2 + Cx_2. \end{aligned} \tag{5}$$

Here subscripts 1 and 2 indicate the first and the second of the two subsystems. All other parameters of the subsystems are identical and fixed at $k = 0.4$, $\alpha = 1.0$, $a = 0.8$, $B = 1.66$ and either $C = 0.591885$ or $C = 0.43924$. The first value of parameter C corresponds to the mode-locked chaotic regimes with rotation number $r = \frac{1}{3}$ and the second value corresponds to the mode-locked chaotic regimes with rotation number $r = \frac{1}{2}$. We will consider the parameters μ and ε as control parameters.

Let us introduce two rotation numbers. One of these represents the ratio between the fast oscillatory modes in the coupled subsystems and the other the ratio between the slow oscillatory modes:

$$r_u = \frac{\langle \tau_{u1} \rangle}{\langle \tau_{u2} \rangle}, \quad r_y = \frac{\langle \tau_{y1} \rangle}{\langle \tau_{y2} \rangle}. \tag{6}$$

These rotation numbers will help us to determine when synchronization occurs between the fast and the slow oscillatory modes, separately.

At the parameter value $C = 0.591885$, the coupled subsystems (4) and (5) individually operate in a mode-locked chaotic regime with the rotation number $r = \frac{1}{3}$. Fig. 8 presents the plots of the rotation numbers for the fast (r_u) and slow (r_y) oscillatory modes of the coupled subsystems (4) and (5) versus the frequency mismatch ε for the value $\mu = 0.035$ of the coupling strength parameter. In this figure one can see an interval of parameter ε values ($0.995 < \varepsilon < 1.005$) where both rotation numbers r_u and r_y are equal to 1. This means that synchronization is observed both for the fast and for the slow oscillatory modes. In Fig. 9, the synchronization regions for the fast and slow modes are plotted separately to allow a more detailed

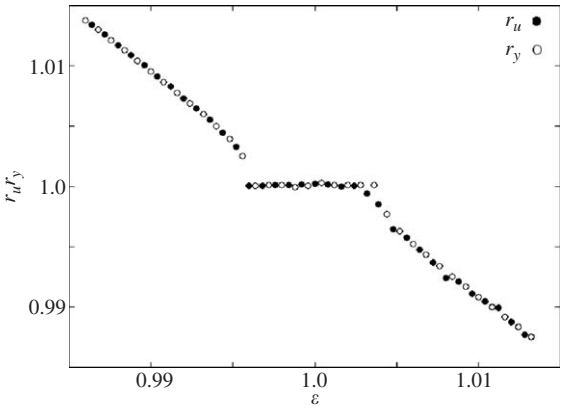

Fig. 8. The rotation numbers r_u and r_y in the coupled systems (4) and (5) as functions of the frequency mismatch ε. $k = 0.4$, $\alpha = 1.0$, $a = 0.8$, $B = 1.66$, $C = 0.591885$, $\mu = 0.035$.

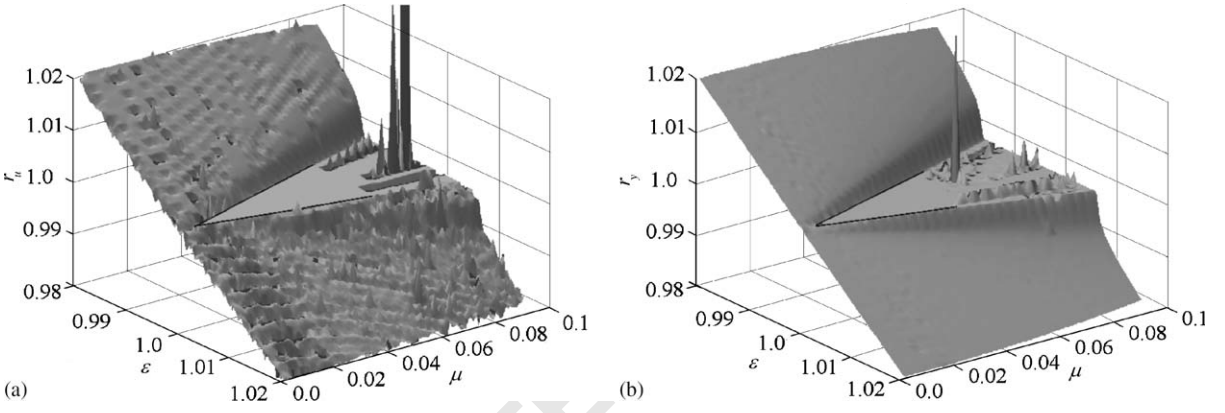

Fig. 9. 3D plots on the parameter plane (frequency mismatch ε–coupling strength μ) for the rotation numbers r_u (a) and r_y (b) in the coupled system (4) and (5). $k = 0.4$, $\alpha = 1.0$, $a = 0.8$, $B = 1.66$, $C = 0.591885$.

visualization of the synchronization picture in the coupled systems. They represent 3D plots of the rotation numbers r_u and r_y versus the parameters ε and μ. One can see synchronization tongues (regions where r_u and r_y are equal to 1) in both figures. Note, that both types of oscillatory modes have nearly identical width of synchronization tongues. Breakdown of synchronization is observed for larger values of the coupling parameter μ, and the rotation number may change abruptly in this region. This is especially obvious for the fast modes of the coupled subsystems (Fig. 9a). For the slow modes (Fig. 9b), these variations are not quite as strong.

A similar situation is observed at the point $C = 0.4392$. In this case, both subsystems show a mode-locked chaotic regime with rotation number $r = \frac{1}{2}$. Fig. 10 presents the plots of rotation numbers for fast r_u and slow r_y oscillatory modes in the coupled subsystems versus the frequency mismatch ε. The coupling parameter is fixed at $\mu = 0.035$. Fig. 11 shows the 3D plots of rotation numbers r_u and r_y versus the parameters ε and μ. Most of the same regularities as in the previous case are observed here too. However, there are some differences. First, a comparison of Figs. 9 and 11 shows, that while the widths of the synchronization tongues for fast (r_u) and slow (r_y) modes are nearly identical in the first case ($r = \frac{1}{3}$), they now have different widths. The synchronization tongue for fast (r_u) oscillatory modes is wider than synchronization tongue for slow (r_y) modes (Fig. 10). Also, the range of parameter μ values, in which synchronization between the subsystems takes place, has now decreased. In the first case both fast and slow oscillatory modes are desynchronized approximately at $\mu \approx 0.06$. Now desynchronization occurs at $\mu \approx 0.04$. This can be explained using the next

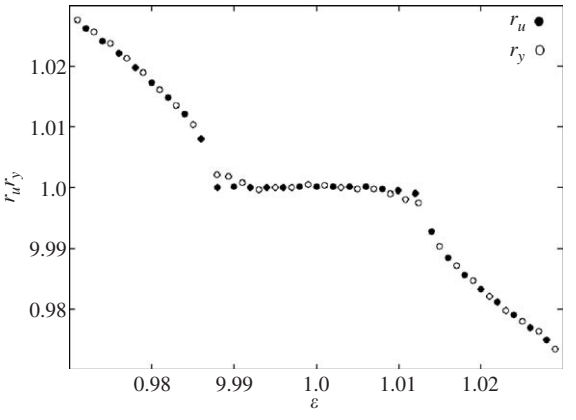

Fig. 10. The rotation numbers r_u and r_y in the coupled systems (4) and (5) as function of the frequency mismatch ε. $k = 0.4$, $\alpha = 1.0$, $a = 0.8$, $B = 1.66$, $C = 0.4392$, $\mu = 0.035$.

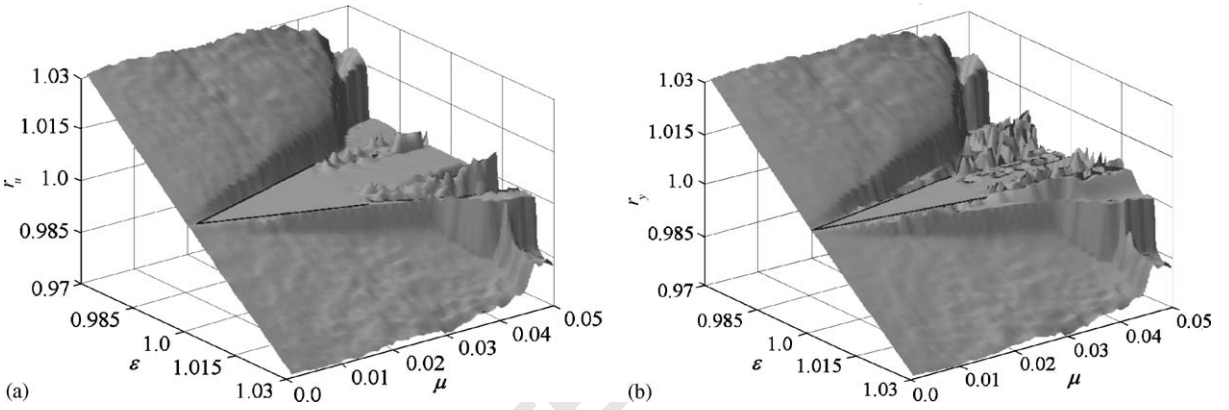

Fig. 11. 3D plots on the parameter plane (frequency mismatch ε–coupling strength μ) for the rotation numbers r_u (a) and r_y (b) in the coupled systems (4) and (5). $k = 0.4$, $\alpha = 1.0$, $a = 0.8$, $B = 1.66$, $C = 0.4392$.

circumstance. The rotation number r is different in the two cases. The first chaotic regime corresponds to rotation number $r = \frac{1}{2}(C = 0.4392)$ and the second chaotic regime corresponding to rotation number $r = \frac{1}{3}(C = 0.591885)$.

Let us finally note that synchronization in the coupled subsystems (4) and (5) is not observed in a case when the parameter C takes value from a vicinity of a point A ($C = 0.4595\ldots$). Rotation numbers r_u and r_y are decreasing passing through the unit value as ε is changing from 0.95 to 1.05 at fixed μ. However, there are no plateaus in the plots of rotation numbers, they demonstrate big jump and decrease in a nonsmooth manner.

4. Conclusion

We considered a simple system with two-mode dynamics and investigated synchronization between the two modes (fast and slow). The individual system consisted of a Van der Pol oscillator coupled to a Duffing oscillator. We showed that there are plateaus on the plot of the rotation number r (the rotation number measures the frequency ratio of the slow and fast oscillatory modes) versus the coupling parameters. Every plateau corresponds to a particular rational value of the rotation number. The system under investigation demonstrates a transition to chaos via the period-doubling bifurcations cascade inside the plateau. Hence, there are mode-locked as well as mode-unlocked chaotic regimes in the system of coupled Van der Pol and Duffing oscillators. Mode-locked chaotic regimes are characterized by a rational rotation number $r = m/n$.

The properties of both types of chaotic regimes have been investigated. The mode-locked chaotic regime is characterized by an attractor with a banded structure. Mode-unlocked chaos, on the other hand, is characterized by a different type of attractor with additional loops inside and around the main body of the attractor and fine additional structure. And these additional loops visited chaotically. This means that the number of fast oscillations per period of the slow oscillations changes chaotically. Thus, the average rotation number of the mode-unlocked chaotic regime is $r \neq m/n$. This is the main difference between the mode-locked and mode-unlocked chaotic regimes.

We have also considered synchronization in a system of two interacting oscillators, each demonstrating two-mode chaotic dynamics. A pair of bimodal oscillators were coupled via their fast variables, and the synchronization properties of the fast and slow oscillatory modes were investigated separately in regions of parameter space where the individual oscillator displayed mode-locked chaos. We demonstrated that synchronization can occur both between the fast modes and between the slow modes, and that the synchronization regimes in the present case are nearly identical. However, the synchronization regime for the fast modes tends to be slightly wider (in terms of the mismatch parameter) than it is for the slow modes. These results are somewhat different from the results obtained by Postnov et al. [27], and we consider this difference to be a consequence of the different coupling structures used in the two studies. It is clear that the tendency of the individual mode to adjust its phase and frequency to an external signal also plays a role. This depends on the strength of the nonlinear interactions. The size and form of the synchronization regions also vary with the internal rotation number of the interacting subsystems. We have seen that the synchronization region can become broader (larger parameter mismatch) and lower (smaller coupling parameter) for larger internal rotation numbers.

Acknowledgments

The study was supported by the European Commision (LSH project No. 005137, BioSim). A.K. and L.T. acknowledge support from the grant CRDF BRHE REC-006 Y2-P-06-13 and grant of RFBR 03-02-16074. L.T. also acknowledges support from the Grant for Modelling and Nonlinear Dynamics (MIDIT) during her visits to Denmark.

References

[1] Y. Kuramoto, Chemical Oscillations, Waves and Turbulence, Springer, Berlin, 1984.
[2] A. Pikovsky, M. Rosenblum, J. Kurths, Synchronization—A Universal Concept in Nonlinear Sciences, Cambridge University Press, Cambridge, 2001.
[3] E. Mosekilde, Yu. Maistrenko, D. Postnov, Chaotic Synchronization: Applications to Living Systems, World Scientific, Singapore, 2002.
[4] L. Pecora, T. Carroll, Phys. Rev. Lett. 64 (1990) 821.
[5] G. Dykman, P. Landa, Y. Neimark, Chaos, Solitons Fractals 1 (1992) 339.
[6] V.S. Anishchenko, T.E. Vadivasova, D.E. Postnov, M.A. Safonova, Int. J. Bifurcation Chaos 2 (1992) 633.
[7] R. Roy, K.S. Thornburg, Phys. Rev. Lett. 72 (1994) 2009.
[8] W. Wang, I.Z. Kiss, J.L. Hudson, Chaos 10 (2000) 248.
[9] N.-H. Holstein-Rathlou, K.-P. Yip, O.V. Sosnovtseva, E. Mosekilde, Chaos 11 (2001) 417.
[10] N.F. Rulkov, M.M. Sushchik, L.S. Tsimring, H.D.I. Abarbanel, Phys. Rev. E 51 (1995) 980.
[11] G. Kolumban, M.P. Kennedy, L.O. Chua, IEEE Trans. CAS 44 (1997) 927.
[12] H. Fujisaka, T. Yamada, Prog. Theor. Phys. 69 (1983) 32.
[13] L.M. Pecora, T.L. Carroll, G.A. Johnson, D.J. Mar, J.F. Heagy, Chaos 7 (1997) 520.
[14] M. Rosenblum, A. Pikovsky, J. Kurths, Phys. Rev. Lett. 76 (1996) 1804.
[15] V.S. Anishchenko, A.N. Silchenko, I.A. Khovanov, Phys. Rev. E 57 (1998) 316.
[16] K.S. Polonsky, B.D. Given, E. Van Cauter, J. Clin. Invest. 81 (1988) 442.
[17] J. Sturis, K.S. Polonsky, E. Mosekilde, E. Van Cauter, Am. J. Physiol. 260 (1991) E801.
[18] I. Atwater, et al., Hormone Metab. Res. 10 (1980) 100.
[19] G. de Vries, A. Sherman, H.-R., Bull. Math. Biol. 60 (1998) 1167.
[20] T.R. Chay, Biophys. J. 73 (1997) 1673.
[21] R.M. Santos, et al., Pflugers Arch. Eur. J. Physiol. 418 (1991) 417.
[22] E. Gylfe, E. Grapengiesser, B. Hellman, Cell Calcium 12 (1991) 229.

[23] M. Barfred, E. Mosekilde, N.-H. Holstein-Rathlou, Chaos 6 (1996) 280.
[24] O.V. Sosnovtseva, A.N. Pavlov, E. Mosekilde, N.-H. Holstein-Rathlou, Phys. Rev. E 66 (2002) 061909.
[25] D.E. Postnov, T.E. Vadivasova, O.V. Sosnovtseva, A.G. Balanov, V.S. Anishchenko, E. Mosekilde, Chaos 9 (1999) 227.
[26] D.E. Postnov, O.V. Sosnovtseva, S.Y. Malova, E. Mosekilde, Phys. Rev. E 67 (2003) 016215.
[27] D.E. Postnov, A.V. Shishkin, O.V. Sosnovtseva, E. Mosekilde, Phys. Rev. E 72 (2005) 056208.
[28] Y. Ueda, Nonlinear Sci. Today 2 (1992) 2.
[29] Y. Ueda, J.S. Thomsen, J. Rasmussen, E. Mosekilde, Math. Res. 72 (1993) 149.
[30] C. Grebogi, E. Ott, J.A. Yorke, Physica D 7 (1983) 181.